Available online at www.sciencedirect.com

ScienceDirect

Procedia Materials Science 9 (2015) 578 – 589

Procedia Materials Science

www.elsevier.com/locate/procedia

International Congress of Science and Technology of Metallurgy and Materials, SAM – CONAMET 2014

Wear analysis of PM compacts with bainitic microstructures, under unlubricated sliding conditions

Ceferino Steimbreger[a]*, Esa Vuorinea[a], Pernilla Johansson[b]

[a]*Luleå University of Technology, Dept. of Engineering Sciences and Mathematics, Luleå, 97187, Sweden.*
[b]*Höganäs AB, Höganäs, Sweden*

Abstract

Ferrous and non-ferrous alloys can be processed by PM. Complex shapes and good surface finishes can be achieved, leading to promising applications, if mechanical properties are demonstrated to be high enough. At the same time, both bainitic and carbide free bainitic microstructures have proved to be excellent candidates for wear applications. Therefore, the aims of this project were steered towards analysing wear behaviour of PM compacts, in relation to their bainitic microstructures.
Three materials were employed and two conditions were taken into account: materials before and after austempering. A reference material was considered, corresponding to Distaloy DC with Mo and Ni. Microstructure was analysed in all the cases by means of optical and scanning electron microscope and it was related to the behaviour observed. Pin on plate reciprocating sliding test without lubricant was utilised in order to measure friction coefficient and specific wear rate in the pins. Effects of alloying elements were also examined.
It was found that austempering decreased impact resistance, but enhanced hardness in Distaloy DC. In contrast, the other two materials presented the opposite behaviour. However, the presence of additional alloying elements in the initial composition fulfilled to increase wear resistance, compared to the reference material. A possible interaction between pores and oxides that may influence wear behaviour was observed. Si allowed carbide free bainitic microstructure to form but heterogeneity could not be prevented. Therefore, the advantage of this microstructure could not be fully used. Results obtained in the present work can lead to new wear applications for PM products, containing bainitic microstructures.

© 2015 The Authors. Published by Elsevier Ltd. This is an open access article under the CC BY-NC-ND license (http://creativecommons.org/licenses/by-nc-nd/4.0/).
Peer-review under responsibility of the Scientific Committee of SAM–CONAMET 2014

Keywords: Carbide Free Bainite, Powder Metallurgy, Reciprocating sliding test

* Corresponding author. Tel.: +54-299-550-098.
E-mail address: cefesteim@gmail.com

2211-8128 © 2015 The Authors. Published by Elsevier Ltd. This is an open access article under the CC BY-NC-ND license (http://creativecommons.org/licenses/by-nc-nd/4.0/).
Peer-review under responsibility of the Scientific Committee of SAM–CONAMET 2014
doi:10.1016/j.mspro.2015.05.033

1. Introduction

Nomenclature

PM	Powder metallurgy
CFB	Carbide free bainite/carbide free bainitic
DC	Material Distaloy DC
M3	Material 3, sintered 48 h
M9	Material 9
BHT	Before heat treatment
AHT	After heat treatment
SWR	Specific wear rate

Bainite discovery can be attributed to Davenport and Bain (1930). They carried out many heat treatments in thin steel specimens. The heat treatment consisted in cooling quickly from austenitizing temperature and then keeping at constant temperature in the range from the lower critical temperature down to room temperature. Hardness, microstructures and other characteristics were analysed and many conclusions were made. In spite of some incongruence in their conclusions (nowadays clarified), this work set a beginning for further studies concerning bainite, since this microstructure exhibited unusual but interesting mechanical properties. It was also one of the first attempts to understand isothermal austenite transformations [Davenport and Bain (1930), Lewis (1929), Robertson (1929)]. From then on, more than eight decades of work have been done in this field and have lead to many important results that are now being intensively used. However, there are many facts that remain to be investigated. Particularly, the present study describes wear behaviour of powder metallurgy produced, bainitic steels.

1.1. Carbide Free Bainite

Silicon is well-known for suppressing carbide formation from austenite, and therefore, making feasible carbide-free microstructures. A Si-content of 1.6 wt% has shown to reduce the rate at which cementite precipitates during tempering of supersaturated martensite in aerospace alloy 300M [Pickering (1979)]. A Si-content of 1.5 wt% hinders the precipitation of carbides in carbon-rich areas formed by carbon partitioned into the residual austenite, and makes retained austenite stable at ambient temperature [Bhadeshia (2001), Caballero et al. (2002)]. The microstructure obtained consists of sheaves of bainitic ferrite and carbon-enriched austenite.

In the past, a complete employment of CFB microstructures could not be achieved because of the incomplete reaction phenomena. Bhadeshia and Edmonds (1983a, 1983b) overcame this difficulty by controlling carbon content and alloying elements, obtaining a fine carbide-free bainitic microstructure that can be transformed at low temperatures.

Aluminium has a similar effect as silicon, but the mechanisms by which it acts have not been deeply studied. Nevertheless, carbide-free microstructures could still be found in steels with no Si or Al [Bhadeshia (2001)].

The unique microstructure achieved with controlled bainitic transformation in certain steels, reveals potential advantages that can be summarised as follows:

- The absence of carbides enhances the resistance to cleavage and void formation.
- Extremely fine ferrite platelets control deformation mechanism and shorten the mean free slip distance.
- Cracks that may propagate through retained austenite suffer a blunting effect produced by the ductile phase. Furthermore, the high stresses developed in the crack tip will induce a TRIP effect that additionally increases the toughness. This stress/strain-induced martensitic transformation enhances the work-hardening capacity of the material, thereby avoiding the usual ductility reduction when refining the grain size.
- TRIP effect can also be useful for parts working in wear conditions.
- Although high solubility of hydrogen in austenite, its diffusion coefficient in that phase is lower than in ferrite. Retained austenite can then increase the stress corrosion resistance.

- Wear resistance under rolling/sliding conditions have shown to be enhanced in carbide free bainitic microstructures [Jin and Clayton (1997), Chang (2005), Leiro et al. (2011)]. Moreover, nanostructured CFB steels have also revealed to accomplish quite good wear properties [Leiro (2012), Yang et al. (2012)].
- Excellent combination of properties obtained in these steels can be achieved with the addition of relatively cheap alloying elements.

However, some undesirable microstructures can be obtained after austempering. *Blocky* austenite can transform prematurely to high carbon martensite under stresses. The resulting phase is untempered, hard and brittle, and it is detrimental to mechanical properties if its presence is large. Blocky austenite formation can be avoided, though, by promoting carbide-free bainitic microstructures. This can be achieved by reducing the austempering temperature for a particular composition and lowering carbon concentration in order to delay austenite enrichment [Bhadeshia and Edmonds (1983a), Bhadeshia and Edmonds (1983b), Bhadeshia (1982)].

1.2. Powder metallurgical produced CFB-steels

All benefits associated to PM products have introduced the possibility of manufacturing carbide free bainitic steels by this method. In addition of resulting in high tolerances, having a high repeatability, and being an economically favourable production method, has the PM production technique by pressing and sintering shown to limit the austenite grain size. The fine sizes obtained delay martensite formation by decreasing Ms, in spite of the carbon content of the steel. Moreover, the high concentration of grain boundary surfaces generates numerous nucleation sites for bainite formation, accelerating thereby the reaction. Low austempering temperatures can be achieved in those conditions, and a nanostructured CFB will form [Lonardelli (2012)].

The high temperature used during sintering enhances the risk of oxidation of alloying elements. In addition, the chemical composition will be different from that of cast or wrought materials. Some elements as Cu, Ni and Mo, which are easily reduced, are commonly employed in powder metallurgy. Vuorinen et al. (2013) have shown that it is possible to form microstructures with large amount of CFB and proposed the development of a new powder based on Fe, Si, Ni and Mn.

Manganese is commonly used in PM products. Its self-cleaning effect during sintering is a result of its high affinity with oxygen and a high vapour pressure. Therefore, an addition of manganese causes that metal to evaporate during sintering. The gas penetrates then into the interconnected pores and pushes out the air or CO_2 that may exist inside them. A portion of manganese vapour escapes to the surrounding sintering atmosphere where it reacts with the oxygen and generates a protective layer. This oxide coating prevents the oxygen to reach the silicon and thereby hinders silicon oxidation [Šalak et al. (2001), Šalak and Selecká (2012)].

2. Materials and experiments

2.1. Chemical composition

Three PM steels were tested, and their compositions and densities are presented in Table 1. As can be seen, Distaloy DC (DC refers to “Dimensional Control”) steel has the lowest amount of alloying elements and is regarded as the reference material. Distaloy DC (from now on, DC) is produced by diffusion bonding 2% nickel to Astaloy Mo (pre-alloyed with 1.47% Mo). This ensures good compressibility and small dimensional scattering [Höganäs (1997)].

Material M3, which is sintered 48h and material M9 were designed with DC as the main powder. In material M3 Si was added as Fe45Si pre-alloyed powder, P as pre-alloyed Fe3P powder and Mn as Fe81Mn powder [Vuorinen et al. (2013)]. Material M9 is a pre-alloyed powder. Graphite and Kenolube were added separately to the powder mixtures.

The three materials were compacted with a pressure of 600 MPa and sintered at 1120°C in N_2H_2 atmosphere. The only difference among them is that M3 was sintered 48h, whereas DC and M9 were sintered during 1h. All samples were austenitized to 860°C for 15 minutes, and then quenched and kept in a salt bath at 250°C for 2 hours. After this treatment specimens were cooled to room temperature in air.

Table 1. Chemical compositions of PM steels.

Material	Density (g/cm3)	Chemical composition (%wt)						
		C	Mn	Ni	Mo	Si	P	Fe
DC	7.07	0.8	-	2	1.47	-	-	95.73
M3	6.56	0.8	2	1.81	1.36	2.47	0.1	91.46
M9	6.71	0.8	2	1.8	1.6	-	-	93.8

2.2. Wear test

For testing wear properties of materials a Cameron Plint apparatus was used, according ASTM G133-02 [ASTM (2010)]. The machine can achieve ball, cylinder or ring on flat, dry/lubricated contact with a reciprocating sliding motion from a lever. 2 tests were carried out during 6 hours for each material and condition. The load, stroke of the pin and frequency were 200 N, 6 mm and 1 Hz, respectively. Making use of the contact area, pressure was calculated to 4 MPa. During testing, room temperature was normally 27°C and maximum temperature reached was 30°C. Relative humidity was around 10% in all tests.

Pins were made of the materials to be tested, with 8mm diameter and 12 mm length. A smooth blunting of the edges was done in all the specimens in order to avoid edge effects during testing that may affect the results.

Plates were manufactured with EN-55Si7 steel, austenitized for 30 minutes at 860°C and then austempered at 300°C for 1 hour. Average hardness was 400 HV. After the heat treatment, the plates were grinded, removing 0.5 mm from each side. Dimensions were set according to the machine holder and the thickness was selected to be 9 mm. Grinding was executed both in the pins and plates up to P2000 abrasive paper, giving roughness less than those required from ASTM G133-02 (0.02-0.05 μm) [ASTM (2010)].

Friction coefficient was calculated as the normal load divided by tangential force. The later was measured with a load cell and processed by software, giving the friction coefficient with time. In general, data is presented as a function of distance. Additionally, specific wear rate (SWR) was determined. It is an expression of the volume lost during the test divided by the load and sliding distance. Volume loss can be calculated from the mass loss and material´s density. In the present work, two SWR were obtained: one using only the weight lost in the pin and its density in order to measure the wear in the pin alone, and another calculated considering both mass loss in the pin and the plate with respective densities. The latter gives an idea of the tribo-par behaviour.

3. Results

3.1. Charpy impact test

Energy absorbed after impact is summarised in Fig. 1 for each material and condition. Note that there is a relevant increase of impact resistance in M9 and to a lower extent in M3. Distaloy DC did not show an improved behaviour after austempering.

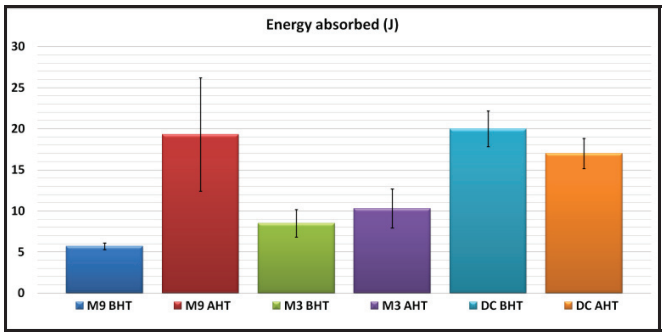

Fig. 1. Charpy impact energy of the tested materials, before (BHT) and after (AHT) heat treatment.

3.2. Fractography

For SEM observation, Charpy impact fracture samples were cleaned with an ultrasonic machine, submerged into ethanol, for 5 minutes. Then, they were dried in a gel mixture for one day.

Samples before heat treatment (BHT) of DC steel presented a mixed mode of fracture containing dimples and feather patterns within some grains, as can be seen in Fig. 2(a). EDS analyses were performed on surfaces showing different fracture behaviours, and a higher amount of Ni was detected in dimpled regions. After heat treatment, DC contained almost no brittle features. This can be observed in Fig. 2(b).

On the other hand, M3 BHT showed mainly brittle fracture with intergranular features, probably due to some contamination, while M3 AHT exhibited a mixed mode of fracture, as it is displayed in Figs. 3(a) and 3(b), respectively.

Likewise, Figs. 4(a) and 4(b) display fracture surfaces of M9 before and after heat treatment, respectively. In the former case, fracture was brittle with preferential failure along prior particle boundary. In contrast, M9 AHT exhibited dimple formation in regions that achieved good bounding from the sintering process. In both cases several "smooth" surfaces were observed that did not show neither dimples nor cleavage or brittle fracture and can be regarded therefore as unbounded regions.

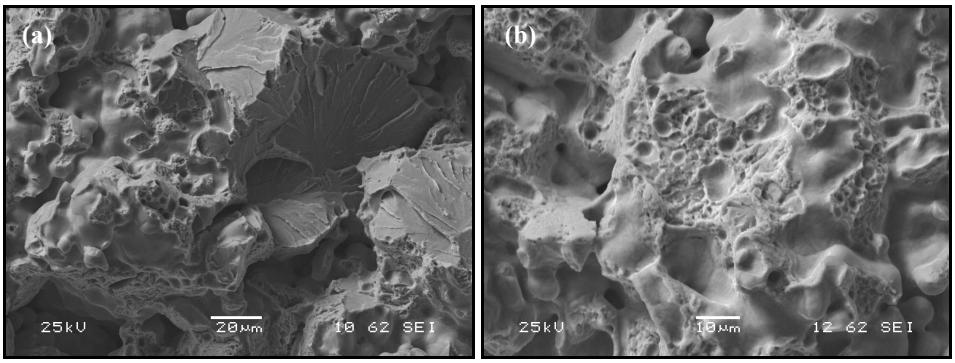

Fig. 2. Fracture surfaces. (a) DC BHT, x700; (b) DC AHT, x1200.

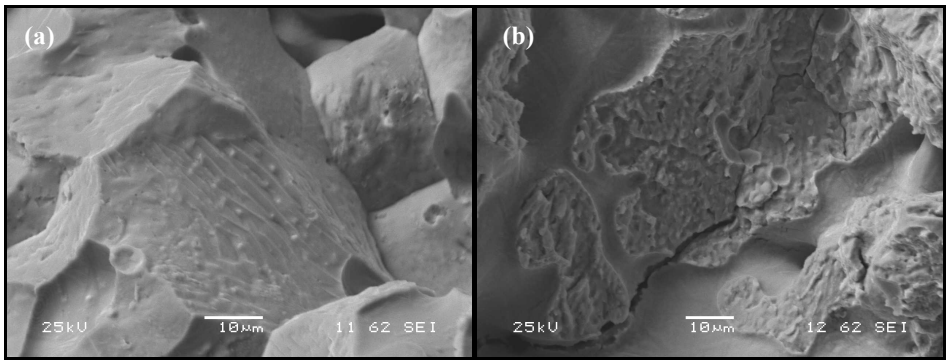

Fig. 3. Fracture surfaces. (a) M3 BHT, x1600; (b) M3 AHT, x1300.

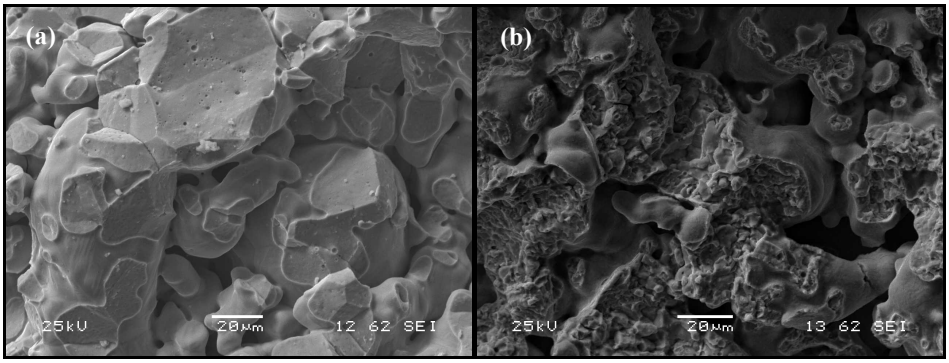

Fig. 4. Fracture surfaces. (a) M9 BHT, x700; (f) M9 AHT, x700.

3.3. Microstructure analysis

After grinding and polishing, cross sections of Charpy bars were etched with Nital 3% and observed in the microscope. The procedure adopted in the present work is distinguishing different kind of microconstituent and identifying them by means of Vickers hardness (100g), SEM and EDS analysis. Results are summarised in Table 2, showing mainly mixtures of bainite (B), retained austenite (RA) and martensite (M) (Note: Relative percentage values are written for those microconstituents that could be isolated up to a certain degree of accuracy). Examples of microstructures encountered in material DC BHT and AHT are illustrated in Figs. 5(a) and 5(b), respectively. Analogously, Fig. 6 displays microstructure in M3 AHT.

Table 2. Microstructures of PM steels.

Material		General microstructure
DC	BHT	Coarse B and islands of Ni-rich RA surrounded by M.
	AHT	8% islands Ni-rich RA and 82% B with different amounts of RA+M.
M9	BHT	B with different amount of RA. Blocky austenite was identified in some regions.
	AHT	Mostly bainitic with hardness varying from 500 to 700 HV0.1, due to different amount and shape of RA.
M3	BHT	RA near pores, a transition with martensite needles and RA, and finally, a mixture of RA, M and B (74%). Different amount of each microconstituent leads to different hardness values
	AHT	B with different amount of RA either in lath or blocky appearance (34%). Mixture of M and RA mostly around pores (25%). Some zones presented possibly CFB (24%).

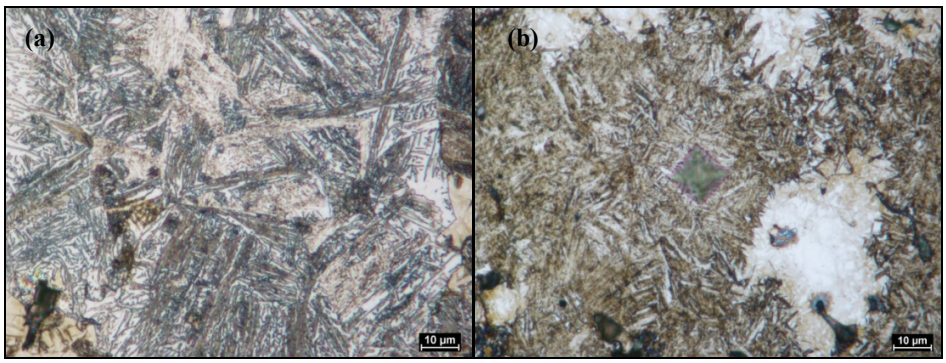

Fig. 5. Microstructures of materials (a) DC BHT, coarse B with RA; (b) DC AHT, fine grained B+M with islands of Ni-rich RA.

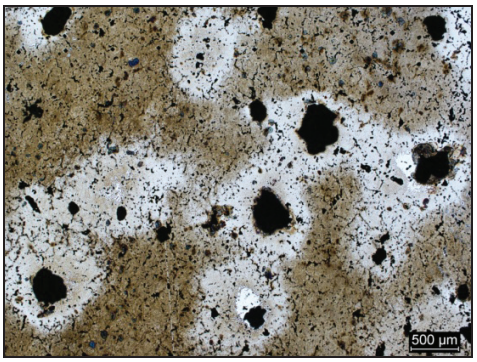

Fig. 6. Microstructures M3 AHT. RA (bright white), possibly CFB (pale white) and mixture of B, M and RA (different beiges).

3.4. Hardness measurements

Hardness measurements were performed in all materials for both conditions. Firstly, two arrays of 40 indentations were made all through the thickness of the sample with 1kg load and a distance of 0.5 mm between each other. Results of these tests are revealed in Fig. 7. Later, sets of minimum 50 indentations were executed with 100g load in order to relate hardness with microconstituents. This assortment of measurements was used to characterise microconstituents found by optical analysis.

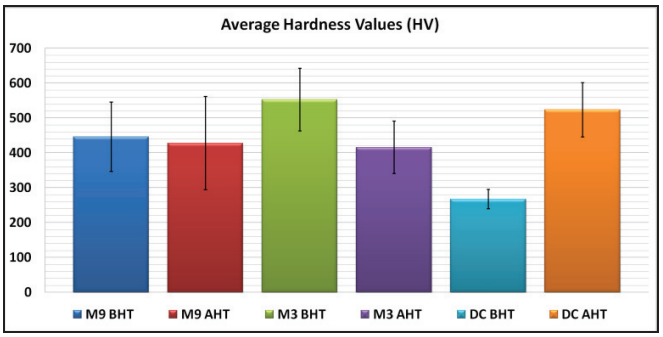

Fig. 7. Average hardness values and standard deviations of the compacts.

3.5. Wear test

Running-in period during wear testing varies widely and depends on the initial roughness and the materials defining the tribo-pair [Van Beek (2009)]. Therefore it is more valuable calculating the average friction coefficients during steady state. This was done for all the cases and results are plotted in Fig. 8. Calculations were made on the base of three measurements. Note that all average values of friction coefficient are gathered in a small range of values from 0.92 to 1.

A combined plot of wear and mechanical parameters provides much information of the wear tests. It was found that highly heterogeneous microstructure is responsible for the variations in average hardness results. In spite of the existence of a microscopic contact area (Real Contact Area in literature [Van Beek (2009), Rabinowicz (1995)]), the hardness values using 1kg load are more suitable for characterizing wear behaviour, since macroscopic damage was observed in all samples after the test (ploughing, cutting, transfer of material through adhesion, etc.). Therefore, plots are referred to HV_1.

Figs. 9(a) and 9(b) show SWRs for both pin and the tribo-pair for 6 hours´ tests. The use of SWR_{pin} is valuable

for comparing directly pins response to wear on the basis that the plate material is the same for all samples, whereas SWR_{total} consider the overall weight loss and is useful in the comparison of the tribo-pairs.

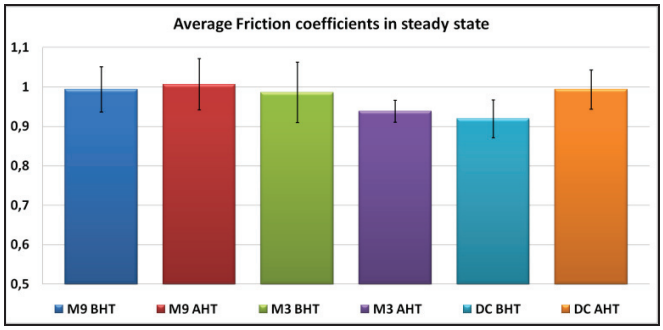

Fig. 8. Average friction coefficient during steady state.

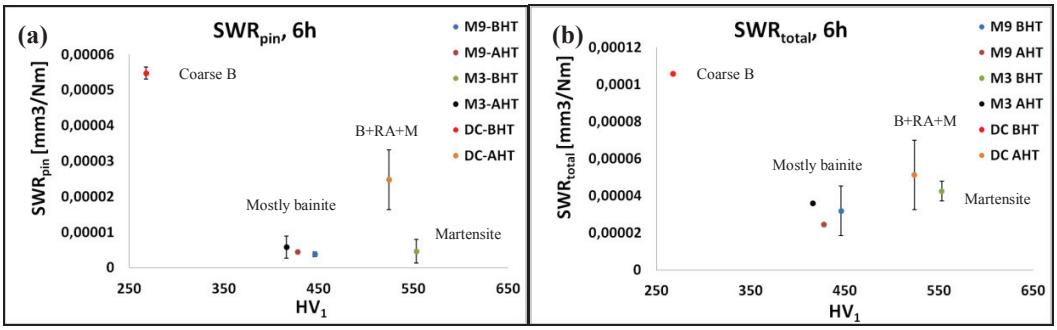

Fig. 9. SWRs vs. HV (1kg), for 6 hours´. (a) pins; (b) pin+plate.

4. Discussions

Impact test results revealed lower values of samples AHT in material DC in comparison with hardness of samples BHT. Moreover, a great dispersion of results can be observed in samples AHT of both M3 and M9. Impact values of BHT samples presented lower scatter in both cases. Although M3 has the lowest density of all tested samples, with higher amount of porosity and larger pore sizes, it did not show the lowest value of energy absorbed. This highlights the importance of alloying elements for the mechanical behaviour of PM compacts.

It is also very important that in M3 and M9, the average energy absorbed is higher in samples AHT than in those BHT, because of austempering. In M9, the effect of heat treatment is more evident. Moreover, lowest impact value of samples AHT is more than twice as high as the greatest value in samples BHT.

Impact results are directly related to microstructures obtained after austempering. Distaloy DC, for example, experienced a transformation from soft microconstituents BHT to harder microstructures like fine bainite. The same was found in M3 and M9, where bainitic microstructures prevailed over the piece, compared to harder microstructures BHT.

Furthermore, it is worth mentioning the importance of porosity as a major detriment to mechanical properties. Sintered microstructures are also known to be inhomogeneous, even in full-density materials fabricated by hot isostatic pressing [Randall (1994)]. Weak links can form due to incomplete diffusional homogenization: frequently, powders like iron, nickel and graphite are mixed before compaction, but homogeneity cannot always be achieved because of the short time at the sintering temperature. Therefore, alloying distribution is uneven and it results in point-to-point composition and microstructural changes. Fracture will preferably occur in those weak links. Although carbon is homogeneously distributed by diffusion during sintering, it can interact with other elements in

highly alloyed regions leading to carbide formations. This uneven carbon distribution has the most remarkable negative effects on uniform strength and must therefore be controlled.

Powder metallurgy deals with particles with different shapes and sizes that can lead to a statistical distribution of both features. In other words, variation in pore distribution and density from sample to sample can be found and can influence results from impact tests. This can explain the scatter found in each material. Likewise, heterogeneous microstructures may have influenced values obtained. It must be considered, however, the statistical nature of the Charpy test, especially when dealing with porous materials and samples that are not V-notched.

Before heat treatment, material DC fractured in a mixed mode, exhibiting both dimple formation and cleavage zones. Fracture path was rather transgranular. Brittle behaviour was associated to large areas, and was not related to particle boundaries, whereas dimples were found in smaller regions or in planes at a high angle to the main tensile stress, i.e. those with a large shear component. Regarding chemical composition, it is possible to believe that zones presenting dimple formation can have higher alloying content, due to heterogeneous distribution of elements during sintering.

Feather markings like the one presented in Figs. 2(a) and 3(a) are fan-shaped arrays of very fine cleavage steps on a large cleavage facet [ASM (1987)]. Lines formed converged to an apex that points back to the fracture initiation in that grain. In material DC, feather patterns were found in most of the cleavage planes, presenting larger cleavage steps than in M3. Apex of the fans usually pointed back to micropores, or other stress concentrators, like sharp edges.

M9 BHT achieved the lowest energy absorbed, in accordance with the extremely smooth fracture surfaces observed. On the other hand, M3 BHT presented a slightly higher impact resistance and its fracture surface showed sharp edges, and smooth features, although rougher than M9 BHT. Both fractures in M9 and in M3 BHT are brittle, assisted by cleavage mechanisms. Fracture path is mostly related to prior particle boundaries, and this can be due to some contaminants present in the compact-sintering process. In this sense, it is important to underline the fact that welded regions between particles are coincident with grain boundaries, as can be seen in Figs. 3(a) and 4(a).

Similarly, fracture surfaces after heat treatment were analysed. Reference material presented good particle binding and better adherence in comparison with M3 and M9. Fracture did not follow preferably prior particle boundaries path and it showed ductile features, as depicted in Fig. 2(b). EDS analyses were carried out in particular spots, revealing a small increase of Ni content on fractured surfaces. This can be thought of a fracture path, in which Ni diffusion was incomplete, but evidences are not enough to attribute fracture to shortage or lack of either Ni or Mo content. In the case of M9, it was found that particles are not completely bound to each other, even after heat treatment, and that a big amount of interconnected pores are visible (Figs. 4(a) and 4(b)). Fracture seemed to occur in a ductile manner, with dimple formation throughout particles, but most frequently in weak unions between prior particle boundaries. M3 improved its impact resistance with austempering. Fracture mode change from entirely brittle to a mixed mode.

Microstructures detected in all materials were in accordance with results from the impact tests and hardness measurements. If austempering resulted in an increase of one parameter, then the other was found to decrease. From the hardness (1kg) point of view, higher standard deviations were found for all materials after heat treatment, but particularly M9 suffered the largest variation. This dispersion is probably due to porosity and presence of hard microconstituent throughout the sample.

High hardness values were detected in samples BHT in both M3 and M9 and are mainly associated with presence of martensite within bainite. Lowest values were found in the case of DC BHT, since its microstructure consisted basically of coarse/soft bainite. Pores underneath indentations may have influenced some hardness measurements. However, the amount of indentations made on samples, more than compensate this problem.

On the other hand, wear tests showed interesting results that can also be related to microstructures. It is important to highlight the fact that pores interact with oxides either accumulating them during the test and stopping damage, or releasing particles that contribute with abrasion. Evidence of both mechanisms was found.

Although standard deviations presented in Fig. 9 were calculated using only two values, results revealed clear differences among materials. It can be pointed out from Fig. 9(a) that heat treatment has almost no effect in SWR_{pin} in M3 and M9, but improves wear behaviour in Distaloy DC, considerably. Furthermore, M3 and M9 achieved best results in comparison to the reference material.

The same analysis can be made when dealing with SWR_{total}. Fig. 9(b) reveals an improvement in wear properties with the heat treatment for the three materials, although in the case of M3 and M9, decrease in SWR_{total} is lower than in Distaloy DC. Again, overall behaviour of alloyed PM products is better than the reference material.

Additional important information is exposed in Fig. 9. First of all, Fig. 9(a) reveals low values of SWR_{pin} for medium hardness. It is also pointed out the main microconstituents encountered in the samples. Note that those materials with mostly bainitic microstructures present good wear properties without the presence of large amounts of hard and brittle microconstituents like martensite. M3 BHT contains mainly martensite and has therefore a low SWR_{pin}, but if toughness is required in a particular application, this is not a convenient choice.

Likewise, soft microconstituents present in reference material in the as-sintered condition (DC BHT) achieve the highest SWR_{pin} in correspondence with its lowest hardness. The mixture of bainite, retained austenite (RA) and martensite (M) obtained after heat treatment in Distaloy DC fulfils hard microstructures, but fails to give as good wear properties as obtained for the materials M3 and M9.

Fig. 9(b) keeps roughly the same distribution as Fig. 9(a), but a higher SWR_{total} for M3 BHT. Taking into account the fact that SWR_{total} contains the pin and the plate weight loss, this chart confirms the advantages of bainitic microstructures regarding wear applications. In other words, M3 AHT, M9 BHT and M9 AHT showed not only the lowest SWR_{pin}, but also the best results in terms of the tribo-pair.

Since results for M3 AHT and M9 AHT are close to each other, no direct conclusion can be made from these figures. A deeper analysis must consider impact resistance, hardness, tensile strength and other parameters depending on each particular application.

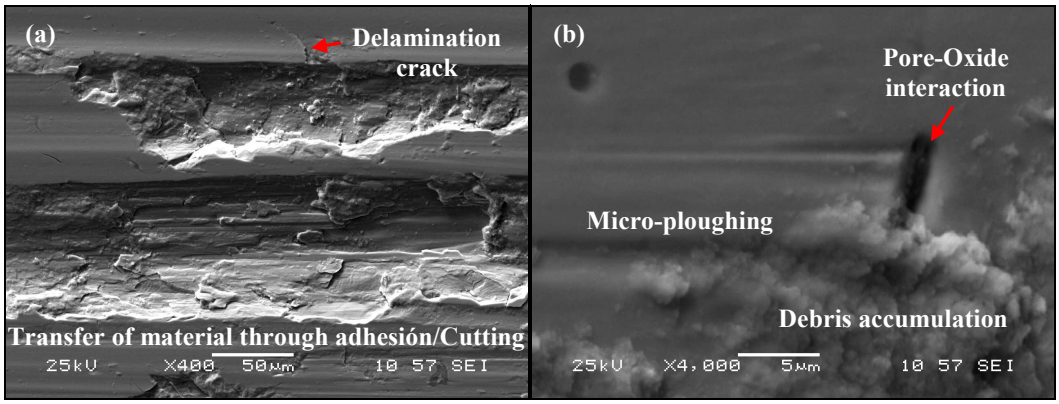

Fig. 10. Worn pin-surface of DC AHT.

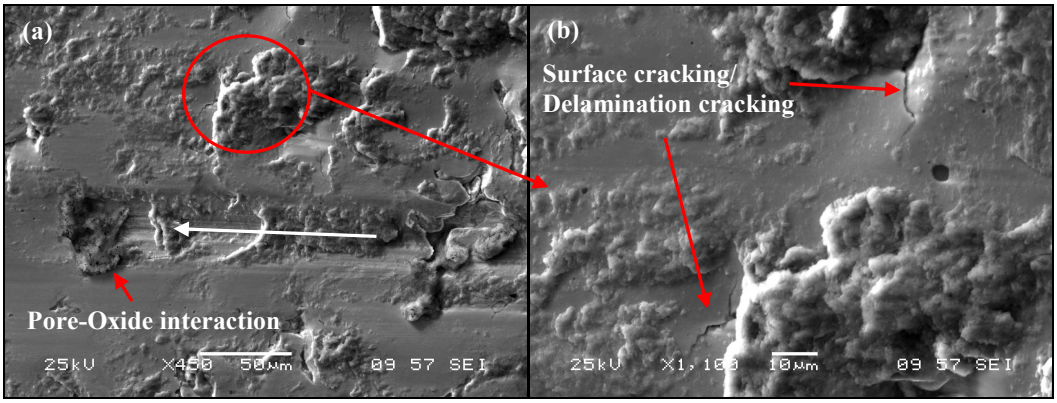

Fig. 11. Worn pin-surface of M9 AHT.

To conclude with wear discussion, it is worthwhile analysing pin´s worn surfaces. Debris accumulation, oxide layer formation, delamination cracks and ploughing were the common mechanisms for all cases

Distaloy DC presented the highest SWR of all materials. Severe damage was observed and was similar to that found in plates. Transfer of material through adhesion is clearly seen in Fig. 10(a). Delamination cracks are also observed, nucleating in regions where material removal was large. Fig. 10(b) reveals a micro-ploughing track ended in an indentation. Oxide debris accumulation is also present.

Material removal by adhesive wear in DC is responsible for its highest weight loss. Additionally, less oxide layers were found on its surface probably due its low content of easily oxidizing alloying elements.

Fig. 11 covers most of the mechanisms found in M9. Fig. 11(a) focuses on debris accumulation and also shows some oxide particles that are gathered into a pore after drawing a track on the pin surface (see white arrow). From this picture, a halt in the abrasive action of oxides is deduced. In Fig. 11(b), a particular region was selected, in which several delamination cracks were found. Delamination cracks are mostly generated from pores, which mean that in this case pores have a negative effect on wear resistance. Continuous wear can leave thin walls in regions hiding pores beneath, and further movement can eventually nucleate cracks. If cracks grow, pieces of material can be removed enhancing 3-body wear. Delamination cracks were also visible in M3 and they nucleated in pores.

Analogously to M9, M3 presented oxide layer formation. Size and stability of oxides revealed that M3 is more prone to oxidation in correspondence with its Si content. It can be thought that this layer prevent base material from wear, since it develops a smooth surface. There is also evidence that debris accumulated inside pores, providing a possible extra benefit of porous surfaces. As was deduced from Table 1, M3 is the most porous material. Therefore, whatever the effect of pores, their influence will be the largest.

5. Conclusions

It has been demonstrated that PM materials present highly heterogeneous microstructures, particularly M3 and DC. M9 was prealloyed and therefore resulted in a more homogeneous microstructure. The presence of a porous structure aids diffusion of Mn in M3, when Mn sublimates during sintering. Therefore, microstructures around pores presented a transition of microconstituents from the pore surface to the core material.

Heat treatment by austempering produces mainly bainitic microstructures in all materials. Distaloy DC presented a mixture of bainite, retained austenite and martensite corresponding to its relative high hardness.

Impact test results showed the largest improvement by austempering in M9, while the Si containing M3 showed only negligible improvement. The formation of CFB is far more important in homogenous materials, such as ADI or wrought Si containing steels. Since M3 BHT presented mainly martensite, HT reduced its average hardness. In contrast, M9 experienced almost no change in hardness. In Distaloy DC the impact resistance decreased and its hardness increased markedly with austempering.

Fracture modes were in accordance with microstructures encountered. Ductile fracture was observed in M9 and DC AHT. M3 presented a fracture path following prior particle boundaries.

All materials experienced ploughing and crack formation in the surfaces after wear test. However, in DC material cracks nucleated from severely worn regions, whereas cracks in M3 and M9 originated from pores.

Oxides either form a coherent and adherent layer, or act as abrasive third particles. Most oxides proceed from the plate. It is clear that pores interact with particles and SEM observations showed that:

- Pores gather particles like oxides or removed material, preventing further damage.
- Particles trapped in pores can be released contributing to wear.

DC AHT presented adhesive wear and less amount of oxide was found, correspondingly with its alloying content in comparison to M3 and M9 alloys. Similarly, M3 developed stable and larger islands of oxide layers. Then, the higher content of easily oxidising elements, the larger the oxide layer formed.

Wear test results support that the addition of Mn and Si to the reference composition improves wear resistance, by the formation of bainitic microstructures.

Bainitic microstructures in M3 and M9 AHT, demonstrated to improve the wear resistance in comparison with the harder DC AHT. Advantages of carbide free bainitic microstructures could not be fully employed because of the heterogeneous microstructure in M3.

A first analysis of mechanical parameters and wear behaviour positions M9 as the best material, with the most convenient combination of properties. HT enhances markedly impact resistance without affecting considerably the hardness. SWR values of M9 AHT showed to be the best together with M3 AHT. However, the latter fail to fulfil a high impact resistance. This can possibly be solved by controlling porosity during sintering.

Acknowledgements

The authors of the present work would like to express their gratitude to Höganäs AB for their support with test materials.

References

American Society for Metals. ASM International. Handbook Committee, 1987. ASM handbook, Vol. 12, Fractography. Metals Park, Ohio: American Society for Metals.

ASTM G133-02, 2010. "Standard Test Method for Linearly Reciprocating Ball-on-Flat Sliding Wear", Annual Book of ASTM Standards, Vol 03.02.

Bhadeshia, H. K. D. H., 1982. Thermodynamic Analysis of Isothermal Transformation Diagrams. Metal Science, 16: 159-165.

Bhadeshia, H. K. D. H., Edmonds, D. V., 1983 (a). Bainite in Silicon Steels: new composition-property approach. Part 1. Metal Science, 17: 411-419.

Bhadeshia, H. K. D. H., Edmonds, D. V., 1983 (b). Bainite in Silicon Steels: new composition-property approach. Part 2. Metal Science, 17: 420-425.

Bhadeshia, H.K.D.H., 2001. Bainite in steels: transformations, microstructure and properties. The University Press, Cambridge, 2nd edition, 432p.

Caballero, F. G., Bhadeshia, H. K. D. H., Mawella, K. J. A., Jones, D. G., Brown, P., 2002. Very Strong Low Temperature Bainite. Material Science and Technology. 18(3): 279-284.

Chang, L.C., 2005. The Rolling/Sliding Wear Performance of High Silicon Carbide-free Bainitic Steel. Wear, 258(5): 730-743.

Davenport, E. S., Bain, E. C., 1930. Transformation of Austenite at Constant Subcritical Temperatures. American Institute of Mining and Metallurgical Engineers 90, 117-144.

Höganäs, 1997. Höganäs Handbook for Sintered Components. Höganäs, Sweden.

Jin, N., Clayton, P., 1997. Effect of Microstructure on Rolling/Sliding wear of low carbon bainitic steels. Wear, 202(2): 202-207.

Leiro, A., 2012. Wear and Fatigue Properties of Isothermally Treated High-Si Steels, Licentiate thesis-Luleå University of Technology.

Leiro, A., Kankanala, A., Vuorinen, E., Prakash, B., 2011. Tribological Behaviour of Carbide Free Bainitic Steel Under Dry Rolling/Sliding Condition. Wear, 273(1): 2-8.

Lewis, D., 1929. The Transformation of Austenite into Martensite in a 0.8% Carbon Steel. Journal of the Iron and Steel Institute 119, 427.

Lonardelli, I., Bortolotti, M., van Beek, W., Girardini, L., Zadra, M., Bhadeshia, H.K.D.H., 2012. Powder Metallurgical Nanostructured Medium Carbon Bainitic Steel: Kinetics, Structure, and in situ Thermal Stability Studies. Materials Science & Engineering A, 555: 139-147.

Pickering, F. B., 1979. Phase Transformations. Institution of Metallurgists, London, series 3, No. 11, 2 VI 7-13.

Rabinowicz, E., 1995. Friction and Wear of Materials. (2nd Ed.). John Wiley & Sons, Inc., NY, USA.

Randall, G. M., 1994. Powder Metallurgy Science (2nd Ed) Princeton, NJ: Metal Powder Industries Federation.

Robertson, J. M., 1929. The Microstructure of Rapidly Cooled Steel, Journal of Iron and Steel Institute 119, 391.

Šalak, A., Selecká, M., 2012. Manganese in Powder Metallurgy Steels. Springer, Cambridge International Science Publishing Ltd. 477 p.

Šalak, A., Selecká, M., Bureš, R., 2001. Manganese in Ferrous Powder Metallurgy. Powder Metallurgy Progress, 1(1): 41-58.

Van Beek, A., 2009. Advanced Engineering Design. www.engineering-abc.com, Netherlands, ISBN-10: 90-810406-1-8.

Vuorinen, E., Vang, J., Carradot, M., Johansson, P., Navara, E., 2013. Powder Metallurgically Produced Carbide Free Bainite. Metallography XV (edited by Margita Longauerová, Pavol Zubko), pp. 480-486.

Yang, J., Wang, T. S., Zhang, B., Zhang, F. C., 2012. Sliding Wear Resistance and Worn Surface Microstructure of Nanostructured Bainitc Steel. Wear, 282-283: 81-84.